Representation of male features in the female mouse Accessory Olfactory Bulb, and their stability during the estrus cycle

Oksana Cohen, Yoram Ben-Shaul[+]

Department of Medical Neurobiology, Institute for Medical Research Israel Canada, Faculty of Medicine, The Hebrew University of Jerusalem, Jerusalem, Israel
+ Corresponding author

Abstract

Most behaviors result from integration of external and internal inputs. For example, social behavior requires information about conspecifics and internal physiological states. Like many other mammals, female mice undergo a reproductive cycle during which their physiology and behavioral responses to males change dramatically: during estrus, they are more receptive to male mating attempts. A critical element in reproductive behavior is the investigative stage, which in mice, and many other species, strongly relies on chemosensation. While the initial approach mostly involves the main olfactory system (MOS), once physical contact is established, the vomeronasal system (VNS) is engaged to provide information about potential partners' characteristics. Given the estrus-stage dependent behavioral response, we asked whether representations of male features in the first brain relay of the VNS, namely, the accessory olfactory bulb (AOB), change during the cycle. To this end, we used a stimulus set comprising urine samples from males from different strains and virility levels, and from estrus and non-estrus females. The stimulus set was designed to reveal if response patterns of AOB neurons conform to ethologically relevant dimensions such as sex, strain, and particularly, male virility state. Using extracellular recordings in anesthetized female mice, we find that most ethological categories contained in our data set are not over-represented by AOB neurons, suggesting that early stages of VNS processing encode conspecific information efficiently. Then, comparing neuronal activity in estrus and non-estrus females, we found that overall, response characteristics at the single neuron and population levels remain stable during the reproductive cycle. The few changes that do occur, are not consistent with a systematic modulation of responses to male features. Our findings imply that the AOB presents a stable account of conspecific features to more advanced processing stages.

Introduction

To efficiently navigate the environment, social animals must derive information about conspecifics, and evaluate it in light of their own state. One notable example is reproduction, which requires coordination of sexual behavior with internal physiology [1, 2]. In mice, females undergo a 4-to-5-day cycle, characterized by hormonal and physiological changes that effect the reproductive system and the females' responses to male stimuli [3, 4]. The cycle includes a fertile estrus/proestrus phase accompanied by receptive behavior towards males, and a non-estrus phase, during which males are avoided [5]. Sexual behavior is often divided into appetitive, consummatory and refractory stages [2, 5], and the appetitive stage can be further divided into detection, approach, and investigation.

In many species, chemosensation is a central sensory modality which plays a key role in social interactions, and is critical during the appetitive stage. In rodents and most vertebrates, information about conspecifics is obtained via two major chemosensory systems. The main olfactory system (MOS) plays many roles, and among other functions is required for social behaviors [6, 7]. The vomeronasal system (VNS) in contrast, appears dedicated to cues from other organisms, and conspecifics in particular [8]. An important functional distinction between the systems involves stimulus uptake. The MOS detects volatile cues, and can thus sense distant objects. During social interactions, it is likely required to decide whether to approach or withdraw. In contrast, the VNS requires physical contact for efficient stimulus uptake [8-10]. Once contact is made, the VNS can provide further information that is needed for more fateful behavioral decisions. Thus, the VNS is particularly important during the investigative part of the appetitive stage [11-13].

The first brain stage of the VNS is the accessory olfactory bulb (AOB), and its principal neurons are known as mitral-tufted cells (AOB-MCs). AOB-MCs represent a key node, as they receive information from vomeronasal sensory neurons (VSNs) and project to downstream limbic stages [8]. Previous studies have shown that AOB-MCs respond to various bodily secretions including feces [14], saliva [15], vaginal secretions [15], and most prominently, urine [16, 17]. These studies also revealed that AOB neurons show differential responses to urine from males versus females [16-18], from mice of different strains [16, 18], and from females in different physiological states [15]. Thus, the AOB provides critical information to guide social decisions, such as required during reproductive behavior.

At the behavioral level, it was shown that female mice prefer male over female stimuli [19-21], dominant over non-dominant males [22], and intact vs. castrated males [23]. Here, to reveal how sensory representations of potential mating partners is represented in the AOB, we applied a stimulus set that includes urine from castrated, sexually naive, and proven-breeder dominant males (**Fig. 1**). These stimuli correspond, respectively, to males that *cannot* breed, *may* be able to breed, and males that have bred successfully. Our stimulus set therefore represents varying levels of virility, allowing us to reveal if AOB-MCs represent male reproductive status.

Differential neuronal responses as a function of some property are often interpreted as "tuning" to it. However, this is unwarranted unless selectivity is demonstrated across a diverse stimulus set, representing multiple sources of variability [24]. For example, to demonstrate that a neuron is tuned to 'dominant males', selectivity should remain across a wide range of stimuli representing different instances

of dominant male samples. Since the range of possible stimuli is unlimited, this goal can never be fully attained. Nevertheless, any expansion of the stimulus set allows a better characterization of response properties. Guided by these considerations, for each male virility state, we applied male urine stimuli from three distinct strains. This not only reduces the risk for misleading strain-specific conclusions, but also allows testing if AOB neurons are tuned to specific ethologically relevant features embedded in our stimulus set. Revealing the response properties of AOB MCs is particularly interesting given their dendritic fields, which can sample multiple glomeruli [25, 26]. This organization could give rise to response profiles corresponding to combinatorial molecular patterns, and hence to ethologically relevant features.

As mentioned above, reproductive behavior requires evaluation of information about potential mating partners in light of the subject's own physiological states. Some studies [27, 28] (but see also [29, 30]) indicate that not only the probability of mating, but even the initial preference towards male stimuli is modulated by the estrus stage. Thus, in the context of female sexual behavior, it is expected that at some stage of processing, neuronal representations of male stimuli would depend on reproductive state. Consistent with this idea, it was shown that neuronal activity and/or connectivity in hypothalamic brain regions change during the female mouse estrus cycle [30-38]. Furthermore, response properties of vomeronasal sensory neurons (VSNs) are also altered during the estrus cycle [39-42]. However, it was not known if and how AOB sensory representations are modulated during the reproductive cycle. To this end, we recorded neuronal activity from naturally cycling female mice and examined how response properties of AOB-MCs change during the cycle. We hypothesized that responses to "virile stimuli" will be somehow amplified during estrus, reflecting heightened sensitivity, or perhaps increased discriminatory ability.

Thus, this study addresses two interrelated goals. First, to reveal how male reproductive status is reflected by AOB neuronal activity. Second, to determine if representation of the males' reproductive state is altered during the course of the estrus cycle.

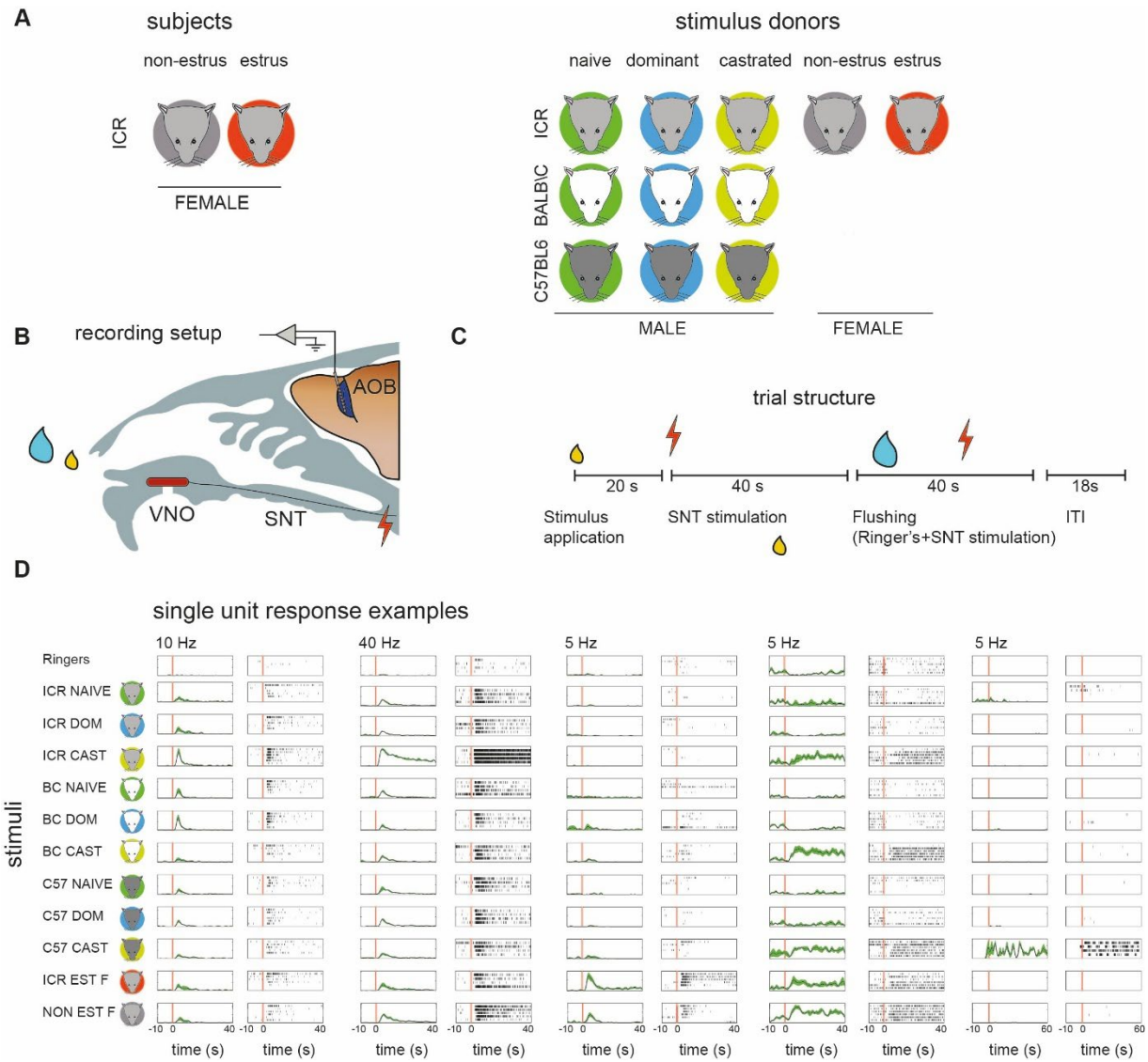

Figure 1. Experimental design and examples of single unit recordings. A. Icons describing the different subject and stimulus donors. Mouse colors denote the strain, while background colors denote the status (estrus, non-estrus for females, naive, dominant, castrated for males). **B.** Schematic off the recording setup. A multisite electrode probe is advanced to the external cell layer of the AOB. Stimuli (yellow drop) are applied to the nostril and, after a delay, the sympathetic nerve trunk (SNT) is stimulated. Between stimulus presentations, the nasal cavity and VNO are flushed with Ringer's solution. VNO: Vomeronasal organ. **C.** Timeline of an individual trial. After a 20 second delay, the SNT is activated to induce VNO activation. Following another 40 seconds, the flushing procedure is initiated. An inter-trial interval (ITI) of 18 seconds is applied between consecutive stimulus presentations. During the experiment, stimuli are delivered repeatedly in blocks. Within each block, each of the individual stimuli are presented in a random order. **D.** Examples of single unit responses to all stimuli. For each unit, responses to each of 11 stimuli are shown. Left panels show the mean firing rate (PSTH, peri-stimulus time histogram), while right panels shown corresponding raster displays. The red vertical line indicates SNT stimulation, except for the unit on the right, where it indicates stimulus application to the nostril. In this specific example, responses began immediately after stimulus application, prior to SNT stimulation.

Results

We recorded stimulus induced responses from the AOB of estrus and non-estrus anesthetized adult ICR female mice (**Fig. 1A, B**). Stimulus presentation includes sample application to the nostril, followed by electric stimulation of the sympathetic nerve trunk, which triggers stimulus uptake by the VNO (**Fig. 1C**). During each session, we repeatedly present one of several stimuli in a pseudorandom order, with each stimulus presented at least four times (see Methods for details). Between consecutive stimulus presentations, the VNO and nasal cavity were washed with Ringer's. The stimulus set includes urine from sexually naive, castrated, and sexually experienced dominant male mice, from each of three strains: BALB/C (BC), C57BL6 (C57), or ICR (**Fig. 1A**). These stimuli span two independent dimensions: male reproductive state, and strain. We also presented urine from estrus and non-estrus ICR females (**Fig 1A**). Response magnitudes were quantified as the baseline-subtracted average firing rate, within a temporal window starting at stimulus application, and ending 40 seconds after electrical stimulation of the sympathetic nerve trunk. Examples of single unit responses are shown in **Fig. 1D.** The dataset includes 241 single units from 21 recording sites from 17 estrus females, and 305 single units from 28 recording sites from 20 non-estrus females.

Population level representations and general response features

Responses from all recording sessions (for both estrus and non-estrus females, n = 546 single units) to each of the stimuli are shown in **Fig. 2A** using a normalized response matrix, with non-significant responses (significance threshold of 0.05 using a non-parametric ANOVA, see Methods) set to 0. As a population, AOB neurons respond to each of the stimuli in the set. To compare population activity patterns across stimuli, we applied the correlation distance metric and classical multi-dimensional scaling. This representation shows that the two female stimuli elicit similar patterns, distinct from all male stimuli (**Fig. 2B**). As for intact male stimuli, the main determinant of response similarity is strain (rather than physiological status): naive and dominant C57 stimuli form one cluster, while naive and dominant BC and ICR males form another cluster. Responses to castrated urine are distinct from male or female induced responses. Yet, here too, ICR and BC castrated urine are closer to each other than to C57 urine.

Note that like all dimensionally reduced representations, the representation in **Fig. 2B** is an approximation. Here, the first two eigenvalues of account for 44.6% of the variance of the original distances (30.4% and 14.2%, respectively for the first and second dimension). Another way to evaluate the representation is via the mean error due to the reduced 2-D representation. Here, it is 0.29, whereas the mean of the original distances is 0.73.

The distribution of the number of effective stimuli per neuron is shown in **Fig. 2C**. Most neurons respond to only one stimulus, although a significant fraction responds to all stimuli. The percentage of neurons with significant rate increases and decreases, for each of the stimuli is shown in **Fig. 2D**. Consistent with previous studies in the AOB, rate increases are far more frequent than rate decreases [43, 44]. Also consistent with other studies, female stimuli activate more neurons than male stimuli [17, 44, 45]. Somewhat surprisingly, yet also consistent with previous work [43], castrated stimuli are at least as effective as intact male stimuli.

Mean response strengths for each of the stimuli across the population are shown in **Fig. 2E**. This value effectively combines the number of responsive neurons, and their response magnitudes. This

representation shows that female and castrated male stimuli elicit the strongest responses. A statistical comparison of response magnitudes is given in **Table 1**.

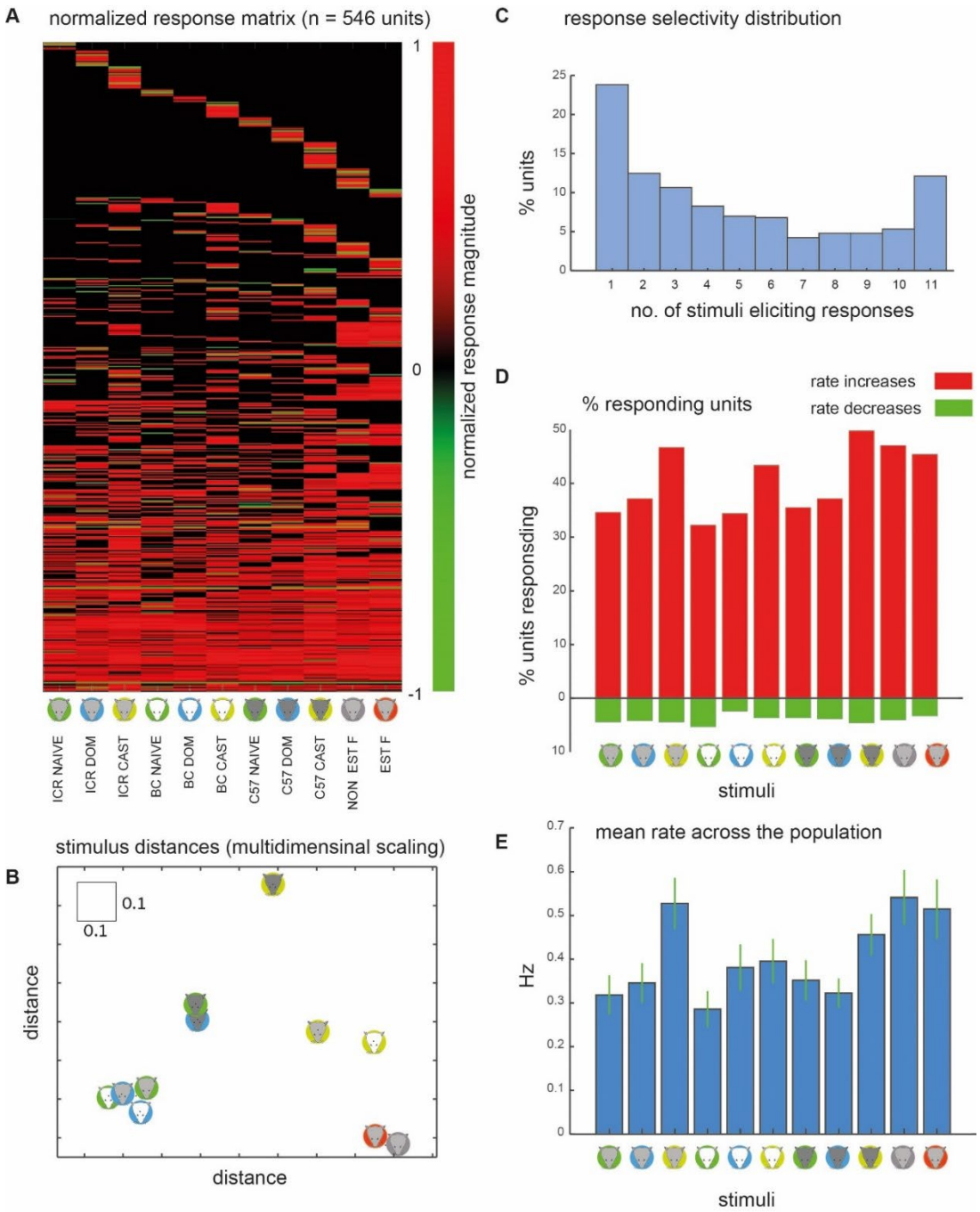

Figure 2. Basic response characteristics. A. Colormap of responses. Each neuron (n = 546) is represented by one row, and each stimulus by one column, as indicated at the bottom. Responses are normalized between -1 and 1. In this representation (and some analyses), non-significant responses are assigned a value of 0. **B.** Classical multidimensional scaling of population level responses using the data shown in panel A and a correlation distance metric. Here, the first two dimensions account for 44.6% of the variability. The mean error due to the reduced 2-D representation is 0.29, whereas the mean of the original distances is 0.73. Note the square indicating a distance of 0.1 for comparison. **C.** Distribution of the number of significant responses across all neurons. **D.** Percentage of neurons responding to each of

the stimuli, separately for rate increases (upper bars, red), and decreases (lower bars, green). **E.** Mean response magnitude, across all recorded neurons to each of the stimuli. Green lines indicate the standard error of the mean. See **Table 1** for statistical comparison of stimulus magnitudes.

Defining response patterns of AOB neurons

To better understand how behaviorally relevant features are represented by AOB neuronal activity, we next examine the response patterns of AOB neurons. Using stimuli from three strains and three male reproductive states, we define patterns corresponding to strain and to male virility status. Our stimulus set contains two female stimuli (estrus and non-estrus ICR urine) which allows us to define additional response patterns corresponding to sex and strain. We define response patterns using relative response magnitude (**Fig. 3A**). For example, to fulfil a *dominant* pattern (DOM in **Fig. 3A**), responses to all *dominant* male stimuli must be stronger than responses to any of the other stimuli. The complementary response pattern (designated as ~DOM) is equally informative. By setting a threshold, neurons with these response patterns suffice to determine if the stimulus source is a dominant male (*given* the present stimulus set). Note also that while we use this approach to define neuronal receptive fields, we are not suggesting that decoding is explicitly achieved in this manner. In addition, we defined "strain adjusted" and "state adjusted" response patterns (an example is shown in **Fig. 3A**). The rationale behind these patterns is that some chemical feature may be modulated by both virility state and by strain. For example, a *dominant strain adjusted* pattern requires that for each strain, the response to the dominant stimulus will be stronger than the responses to the other stimuli *from the same strain*. Here too, we also considered complementary patterns, as they are also informative. We note that criteria for adjusted patterns are less stringent than for the standard patterns. Furthermore, some patterns are not mutually exclusive, and thus, a neuron may fulfil more than a single pattern.

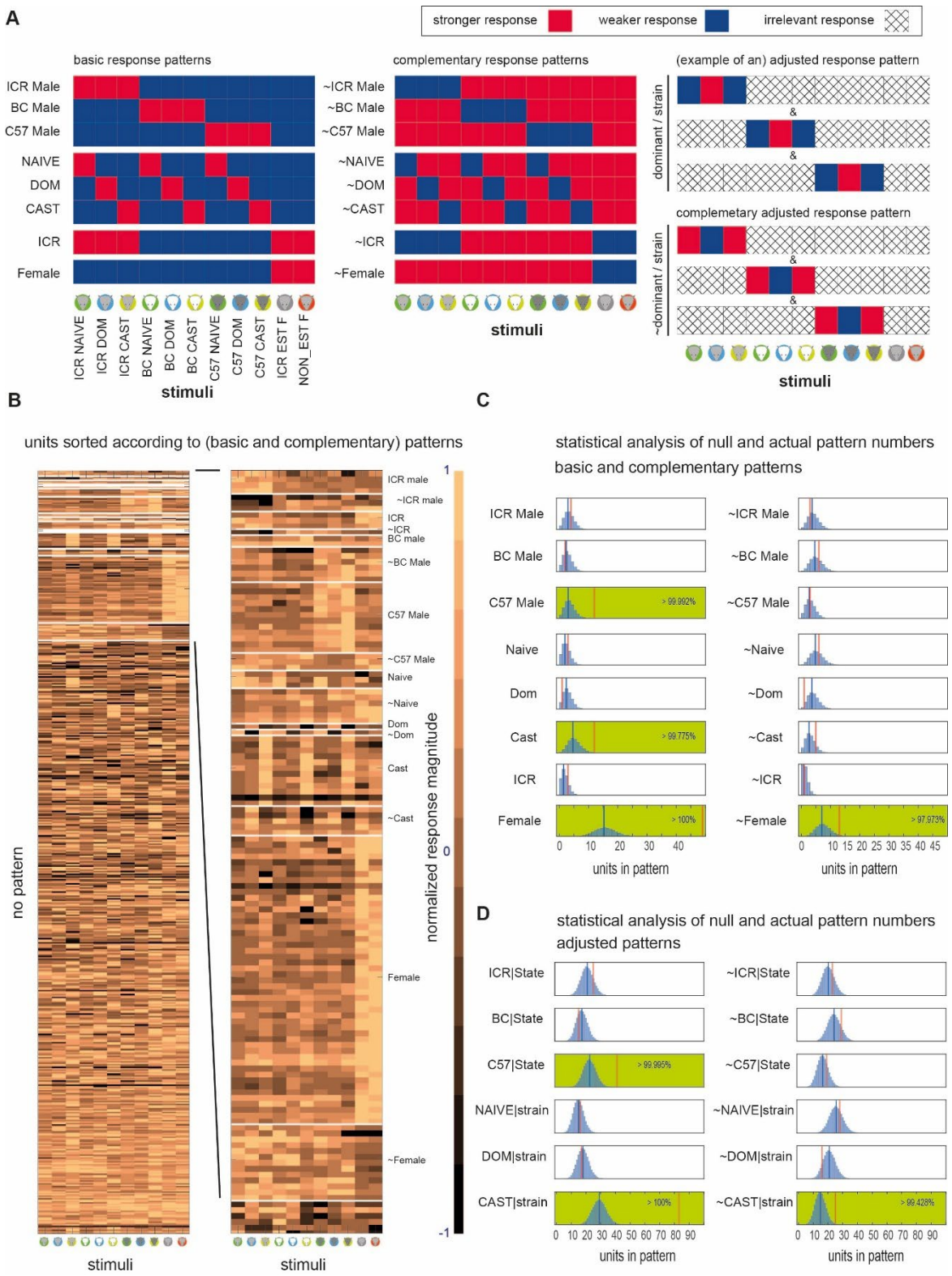
A
stronger response
weaker response
irrelevant response
basic response patterns
complementary response patterns
(example of an) adjusted response pattern
ICR Male
BC Male
C57 Male
NAIVE
DOM
CAST
ICR
Female
~ICR Male
~BC Male
~C57 Male
~NAIVE
~DOM
~CAST
~ICR
~Female
dominant / strain
complemetary adjusted response pattern
~dominant / strain
ICR NAIVE
ICR DOM
ICR CAST
BC NAIVE
BC DOM
BC CAST
C57 NAIVE
C57 DOM
C57 CAST
ICR EST F
NON_EST F
stimuli
B
units sorted according to (basic and complementary) patterns
no pattern
normalized response magnitude
1
0
-1
ICR male
~ICR male
ICR
~ICR
BC male
~BC Male
C57 Male
~C57 Male
Naive
~Naive
Dom
~Dom
Cast
~Cast
Female
~Female
C
statistical analysis of null and actual pattern numbers
basic and complementary patterns
> 99.992%
> 99.775%
> 100%
> 97.973%
units in pattern
D
statistical analysis of null and actual pattern numbers
adjusted patterns
ICR|State
BC|State
C57|State
NAIVE|strain
DOM|strain
CAST|strain
~ICR|State
~BC|State
~C57|State
~NAIVE|strain
~DOM|strain
~CAST|strain
> 99.995%
> 100%
> 99.428%

Figure 3. Analysis of response patterns. A. Graphical representation of response pattern definitions. To fulfill a pattern, each of the stimuli indicated in red should elicit a stronger response than each of the stimuli shown in blue. The left and center panels show the basic response patterns and their complementary patterns, respectively. The panels on the right provide two examples of adjusted response patterns. For example, a dominant/strain pattern requires fulfilment of three conditions, so that within each strain, responses will be strongest to the dominant stimulus. Within a given condition, hatched squares indicate stimuli that are irrelevant for the pattern in question. The complementary adjusted responses patterns are not shown. **B.** All response patterns across neurons. Note that a neuron may fulfill more than one pattern and thus may appear in more than one row. The right panel provides an expanded view of some response patterns. The adjusted categories are not shown in this representation. **C.** Frequency analysis of each of the basic and complementary response patterns. The response pattern name is indicated next to each panel. Within each panel, the blue histogram shows the shuffled distribution of pattern frequencies (n = 100,000 shuffles). The vertical blue lines show the mean value of the shuffled distribution. Red vertical lines indicate the actual number of observed patterns. Green shaded panels indicate significant cases (i.e., the estimated probability to obtain the observed number of cases by chance is less than 5%). In most cases, the probability is considerably lower (as indicated by the numbers within each panel). **D.** Like C for adjusted patterns.

Most response patterns are not over-represented

Responses of single neurons, sorted according to response types are shown in **Fig. 3B** (only basic and complementary response patterns are shown). The image shows that most neurons do not conform to any of the response patterns (78%, 433 of 557 total patterns; note that the number of patterns exceeds the number of neurons since a given neuron may conform to more than one pattern). While some patterns (e.g., *female*) are frequent, others are associated with only a few neurons (e.g., *naive* and *dominant* patterns). However, to gain insight about the sampling properties of AOB neurons, we asked which patterns are represented more than expected by chance. Here, chance implies that responses to each of the stimuli are independent of each other. Practically, we apply bootstrapping (with n = 100,000 shuffles, see Methods) to derive the frequencies for each of the patterns by chance. Bootstrapped distributions and the actual number of observed neurons for each of the patterns are shown in **Fig 3B**. Considering basic and reverse patterns, we find that *female*, *~female*, *C57 male*, and *castrated* are over-represented ($p < 0.05$, **Fig. 3C**). For strain adjusted or state adjusted patterns (**Fig. 3D**), we find over representation of *C57/state*, *cast/strain* and *~cast/strain*. Note that the observed frequencies are determined by the chemical profiles of the stimuli and the sampling properties of neurons. This idea and its implications are further developed in the Discussion. Presently, we note that most of the male strain specific patterns, and the male-virility-state patterns are *not* more frequent than expected by chance.

Neuronal representations are broadly stable over the estrus cycle

We next compare response properties of AOB neurons under the estrus and non-estrus states, beginning with examination of responses at the population level. **Fig. 4A** shows neuronal responses partitioned according to the estrus state of the subject (the same data as **Fig. 2A**). Each pair of stimuli (i.e., each pair of columns within the matrices in **Fig. 4A**) is associated with a distance, which we quantify using two common distance metrics: correlation and Euclidean. Our 11-stimulus set yields 55 pairwise distances, which together provide a measure of representational space. The distance matrices for both states are shown in **Fig. 4B** (correlation distance), and **Fig. 4C** (Euclidean distance). Next, we compare the distances under both states for both metrics (**Fig. 4D**, **E**).

We first note that distances are generally larger during non-estrus, suggesting enhanced discrimination during this stage. However, further analyses of sparseness and selectivity do not support this idea (see below). Furthermore, we note that both Euclidean and correlation distances generally depend on sample

size. In both cases, distances are expected to increase as a function of sample size, which in our dataset, is larger for the non-estrus (n = 305) as compared to the estrus (n = 241) neurons. Because of this factor, we focus here on the similarity of the *relative* within-state distances across the states (and not on their absolute magnitudes). Specifically, we find a positive and significant correlation among pairwise population distances under the two states. Thus, at the population level, representational space remains broadly stable across the estrus cycle. Nevertheless, several points in **Fig. 4D, E** clearly diverge from a linear relationship, implying that representational space differs under the two states. We next examine such state-dependent changes in more detail.

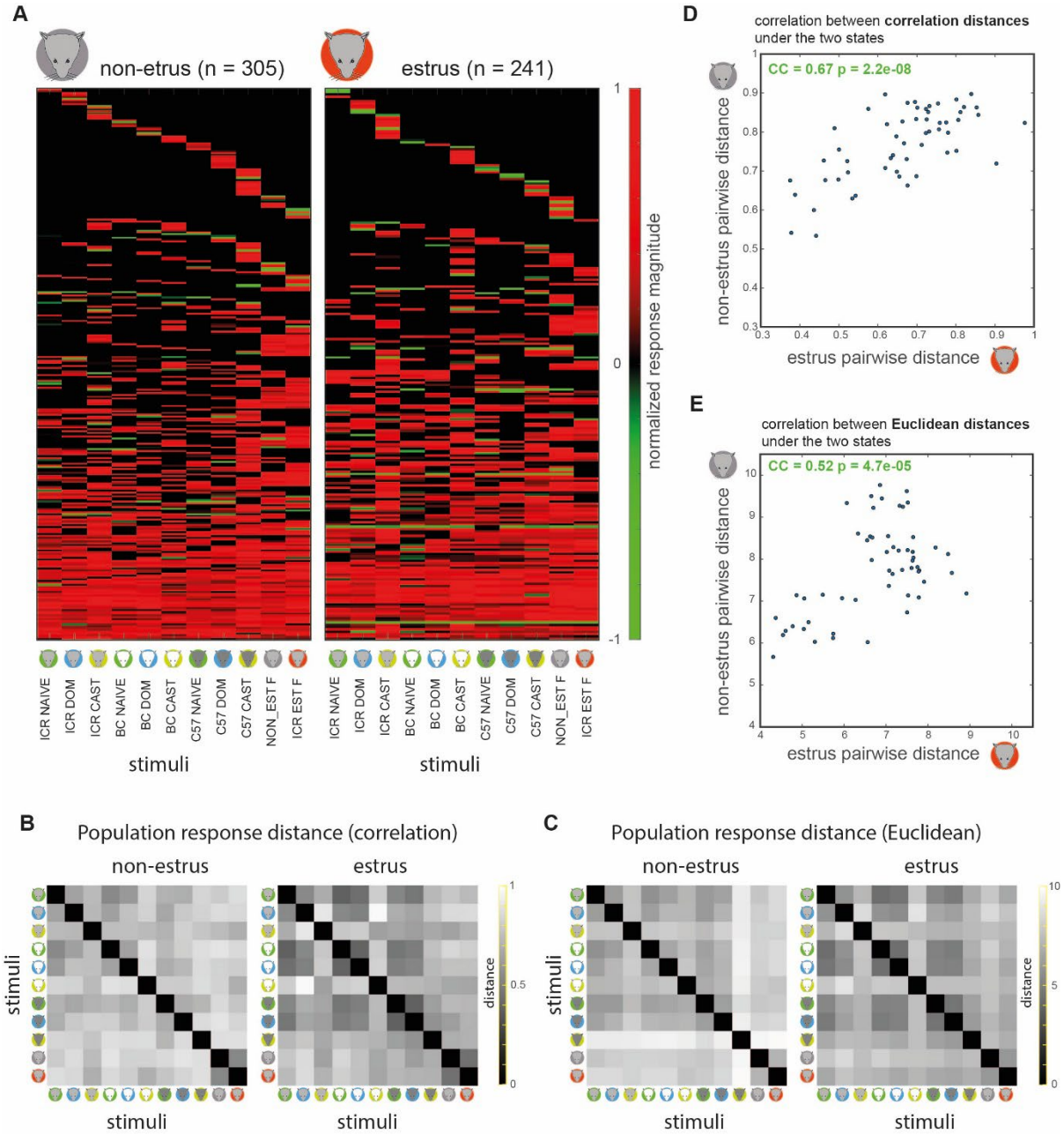

Figure 4. Comparison of population level representations in estrus and non-estrus females. A. Responses of individual neurons. Same data as in **Fig. 2A**, divided by reproductive states. **B.** Pairwise population responses distances in non-estrus (left) and estrus (right) using the correlation distance measure. Each pixel represents the distance between two columns within a given matrix from panel A. By definition, these matrices are symmetric around the diagonal. **C.** Same as B, using the Euclidean distance measure. **D.** Correlation of population level pairwise distances across the two reproductive states, using the correlation distance measure. **E.** Same as in D using the Euclidean distances. In both D and E, the correlation coefficient (CC) and the probability to obtain it by chance (p-value) are indicated within each panel.

Response intensity of most stimuli is stable across the estrus cycle

We next examine the intensity of specific stimuli across the cycle. Specifically, we ask if stimuli associated with virile males elicit stronger responses during estrus. For each stimulus, and both states, we quantify

response magnitudes using the fraction of responsive neurons, and the mean response strength across the population. We compare the fraction of responses (**Fig. 5A**) using a binomial exact test, and the mean response strength (**Fig. 5B**) using one-way non-parametric ANOVA. After (Bonferroni) correction for multiple comparisons, the only significant difference is that during estrus, the *fraction* of responsive neurons to castrated BC male urine increases. There are no significant differences in response *magnitude* to any of the stimuli. Consistent with this, a two-way ANOVA with stimulus and state as factors indicates that the only significant factor is stimulus (p-values were 1.5×10^{-5}, 0.7688, and 0.8193 for stimulus, state, and stimulus x state interaction, respectively). Thus, we conclude that there is no consistent change in response strength across the estrus cycle, and particularly, no increase in response efficacy of stimuli associated with higher virility.

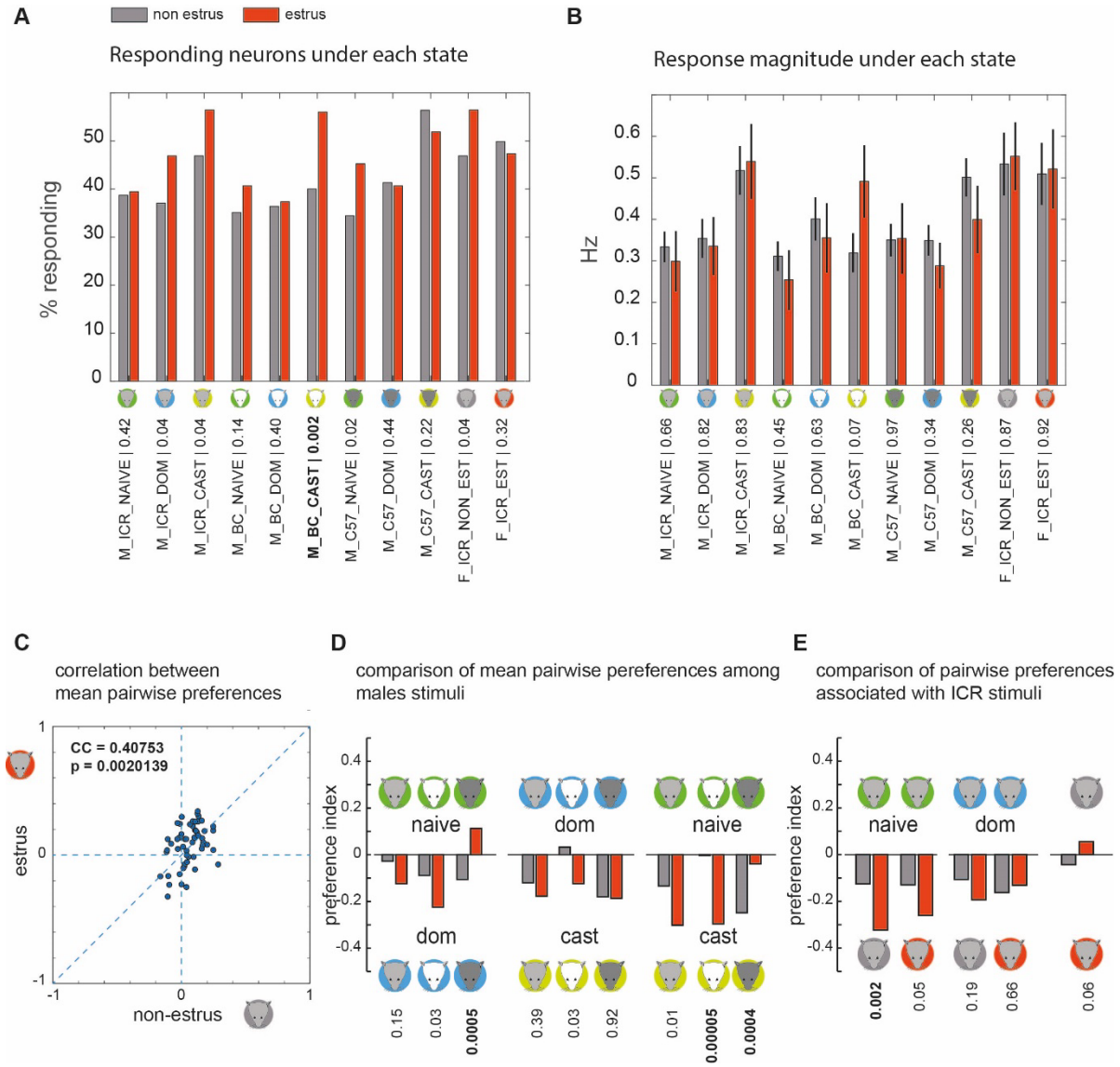

Figure 5. Comparison of responses in estrus and non-estrus females. A. Percentage of responding neurons to each of the stimuli in non-estrus (gray) and estrus (red) neurons. p-values correspond to the binominal exact test. **B.** Mean response magnitude to each stimulus under the two states. p-values correspond to non-parametric ANOVA. In both A and B, the Bonferroni adjusted p-value given 11 comparisons, at the 0.05 level, is 0.0045. The single significant difference is indicated in bold. In A and

B, n = 305 non-estrus, and n = 241 estrus. **C.** Correlation between mean pairwise preference indices under the two reproductive states. The correlation coefficient and the probability to obtain it by chance are indicated. **D.** Comparison of pairwise preference indices under the two states. Each pair of bars corresponds to one comparison. The stimuli are indicated by the icons and text. For example, the first pair of bars on the left corresponds to pairwise comparison of dominant and naive ICR male urine. In both estrus states, there is a stronger response to the dominant stimulus as indicated by the downward pointing bars. However, the difference is not significant. **E.** Comparison of pairwise preference indices between stimulus pairs comprising male and female stimuli. In D and E, significance is determined using a shuffling test (n = 100,000). Bonferroni adjusted p-values at the 0.05 level are 0.0056 and 0.01 for D, and E, respectively. Significant differences among the states are indicated in bold. Note that in most cases, significant differences correspond to cases where responses during estrus are stronger to the *less* virile male stimulus.

The relative magnitude of response strengths remains stable across the estrus cycle

Although our previous analyses ruled out state dependent changes in absolute response magnitudes, they did not directly test changes in *relative* response magnitude. For example, the relative strength of responses to dominant and naive stimuli might change as a function of the estrus state. To explore this scenario, and other related scenarios, we defined a preference index: $PI_{AB} = (R_A-R_B) / (R_A + R_B)$, where R_A and R_B are the responses to stimulus A and B, respectively. PI_{AB} ranges between -1 (exclusive response to stimulus B) and 1 (exclusive response to stimulus A). After calculating these values for each neuron, we obtained their means across the population, and compared them (55 preference indices, defined by our 11 stimuli dataset) under both states. The comparison (**Fig. 5CB**) reveals a positive (0.41) and significant (p = 0.002) correlation between the two states.

Despite the similarity, some pairwise indices change and even reverse signs across the states (as indicated by points located in the upper-left and lower-right quadrants of **Fig. 5C**). To reveal if these reflect meaningful changes in responsiveness to *male* features, we examined pairwise indices associated with virility levels. To account for strain related effects of response strength, we applied this analysis to each strain separately. Significant changes in preference are indicated by bold font in **Fig. 5D** (non-parametric ANOVA, Bonferroni corrected p-value for a nominal level of 0.05 is 0.0056). Significant changes include stronger responses to naive urine during estrus (C57), and two changes involving naive and castrated stimuli (BC, C57), yet in opposite directions. Summarizing, we find no consistent trends across the three strains, and specifically, no evidence for enhanced responses to virile stimuli during estrus.

A related possibility is that during estrus, responses to male stimuli will become stronger relative to female stimuli. To test this, we compared responses between female and (non-castrated) male stimuli from the ICR strain. In all cases (**Fig. 5E**), female urine elicits stronger responses than male urine. The only significant difference (p=0.0024, Bonferroni corrected p-value: 0.01) is that during estrus, responses to non-estrus female urine increase relative to naive male stimuli. Relative response strengths to estrus and non-estrus female urine also did not change during the estrus cycle (**Fig. 5E**). In conclusion, relative response magnitudes are broadly conserved across estrus states. The changes that do take place do not reflect systematic modulation of sensitivity to particular virility states.

Increased selectivity during estrus, but no consistent changes associated with virility state

Thus far, we examined hypotheses related to response magnitudes, reasoning that changes in physiological state can enhance responses to selected stimuli. Yet, another possibility is that individual neurons will become more *selective* to particular stimuli, without necessarily altering response

magnitudes across the population. We first address this issue by examining lifetime sparseness, a normalized measure of selectivity based on response strength, ranging between 0 (uniform response magnitude), and 1 (exclusive response to one stimulus). As shown in **Fig. 6A**, the sparseness of the population is higher for estrus neurons ($p = 0.0079$, Kruskal-Wallis non parametric ANOVA). To determine if these changes reflect selectivity to particular virility states, we examined them directly. Again, to account for potential strain specific effects, we conducted this analysis for each strain separately. In the triangle plots [46] of **Fig. 6B**, vertices correspond to virility states, and dots represent the *relative* response magnitude of individual neurons to each virility state. Thus, dots near the center represent non-selective neurons, while selective neurons are represented by dots near vertices. The plots show that across all strains, dots corresponding to estrus and non-estrus neurons overlap widely.

To determine if selectivity changes with reproductive state, we calculated a response selectivity score [46], for each neuron for each strain. The selectivity score ranges between 0 (uniform response strength) and 1 (exclusive response to one stimulus). We had hypothesized that during estrus, selectivity among male stimuli will be enhanced. This hypothesis appears true for ICR male stimuli, with a small yet significant increase in selectivity during estrus ($p = 0.0017$, Kruskal-Wallis test). However, this is not the case for BC and C57 derived stimuli (**Fig. 6C**), and is thus not a general feature of the estrus state.

Next, we analyzed pairwise response selectivity, by considering, for each neuron, the *absolute* value of the preference index (see Methods), which ranges between 0 (equal responses to both stimuli), and 1 (response to only one of the stimuli). We then compared the distributions of these indices across the two estrus states. The analysis (**Table 2**) is also not consistent with increased acuity for reproductively relevant cues during estrus. For example, of all pairwise comparisons involving a dominant and non-dominant stimulus donor from the same strain, the only significant change involves a *decrease* in selectivity among dominant and naive C57 male urine during estrus. The pairwise comparisons (**Table 2**) also imply that the observed changes for the three-way comparisons for ICR stimuli mostly result from increased selectivity to castrated urine. In summary, while as a population, AOB-MCs from estrus females show somewhat sparser responses, there are no consistent shifts in selectivity for male virility state.

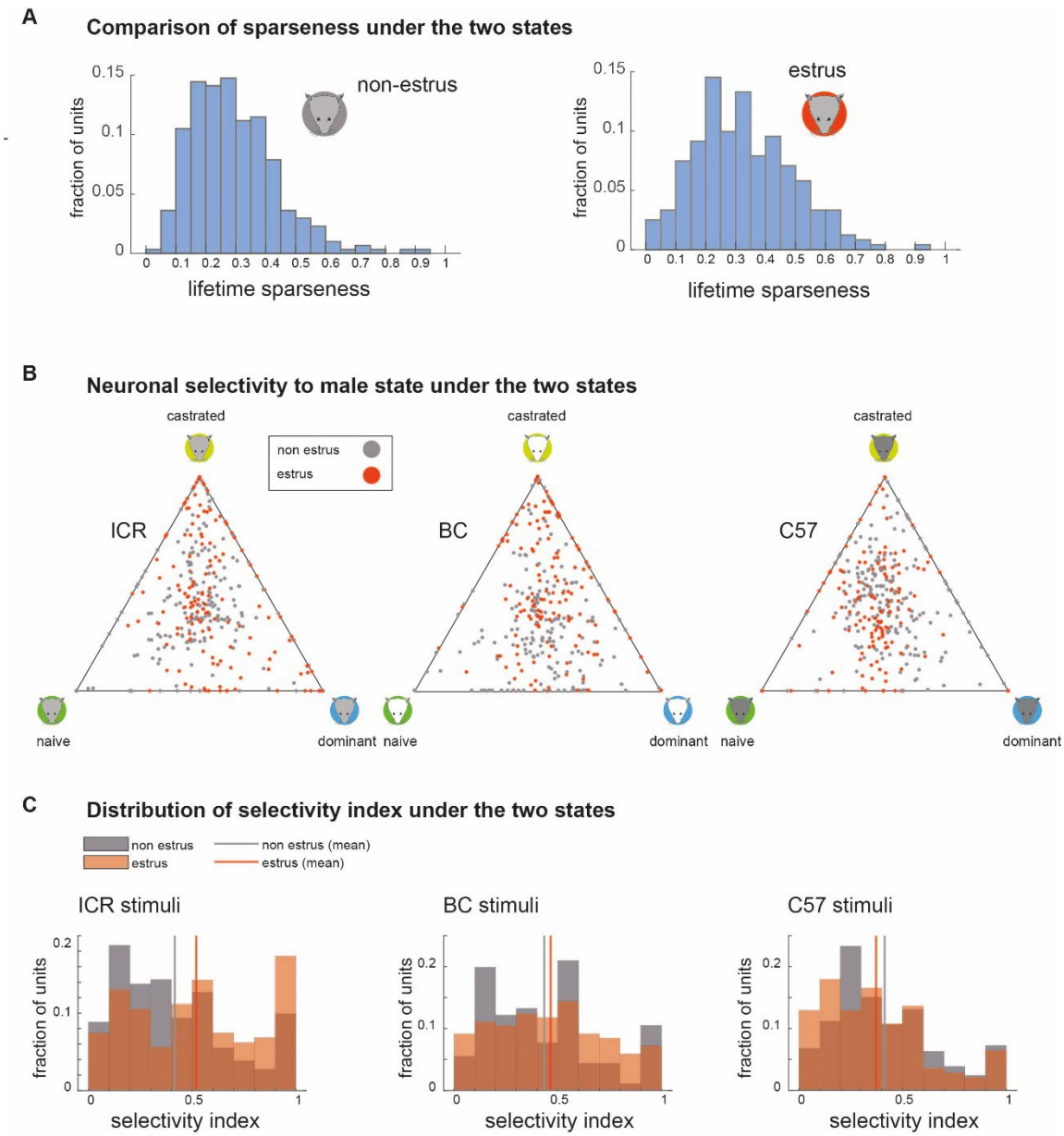

Figure 6. Response selectivity under the two reproductive states. A. Lifetime sparseness distributions for non-estrus (left, n = 305, mean: 0.29 median: 0.27), and estrus (right, n = 241, mean: 0.33, median: 0.31), neurons. Non-parametric ANOVA p-value: 0.0078, reflecting higher selectivity during estrus. **B.** Triangle plots showing relative response magnitude to stimuli from each of the three male states, separated according to strains. Neurons recorded in non-estrus and estrus females are indicated in gray and red, respectively. **C.** Distributions of the male state selectivity index (calculated from the data shown in B) under the two reproductive states, calculated for each strain separately. p-values corresponding to non-parametric analysis of variance (Kruskal Wallis test): (ICR: KW p: 0.0017, BC: KW p: 0.24, C57: KW p: 0.08). Higher selectivity during estrus is observed for the stimuli from ICR male mice (p = 0.0017). Mean selectivity scores: ICR: estrus: 0.52, n = 161, non-estrus: 0.42, n = 181. BC: estrus: 0.47, n = 153, non-estrus: 0.43, n = 181. C57: estrus: 0.37, n = 139, non-estrus: 0.41, n = 206.

Neuronal receptive field distributions across the estrus cycle

Finally, we return to examine response patterns, and compare their frequencies across the estrus cycle. Such changes, if exist, could reflect shifts in tuning properties that would not necessarily be revealed by

our previous analyses. Response pattern frequencies for units recorded in estrus and non-estrus females, for the basic and adjusted patterns are shown in **Fig. 7A, B.** Applying a binominal exact test (see Methods), and correcting for multiple comparisons, none of the patterns show a significant state-dependent difference in frequency. After relaxing significance criteria (by removing the multiple comparisons correction), three differences emerge (bold labels in **Fig. 7**). Again, however, none of these changes suggest an obvious ethological function, and particularly no changes in representation of dominance. In summary, response pattern distributions remain stable during the cycle, and the few changes that do occur, are not compatible with enhanced selectivity to reproductively relevant stimuli.

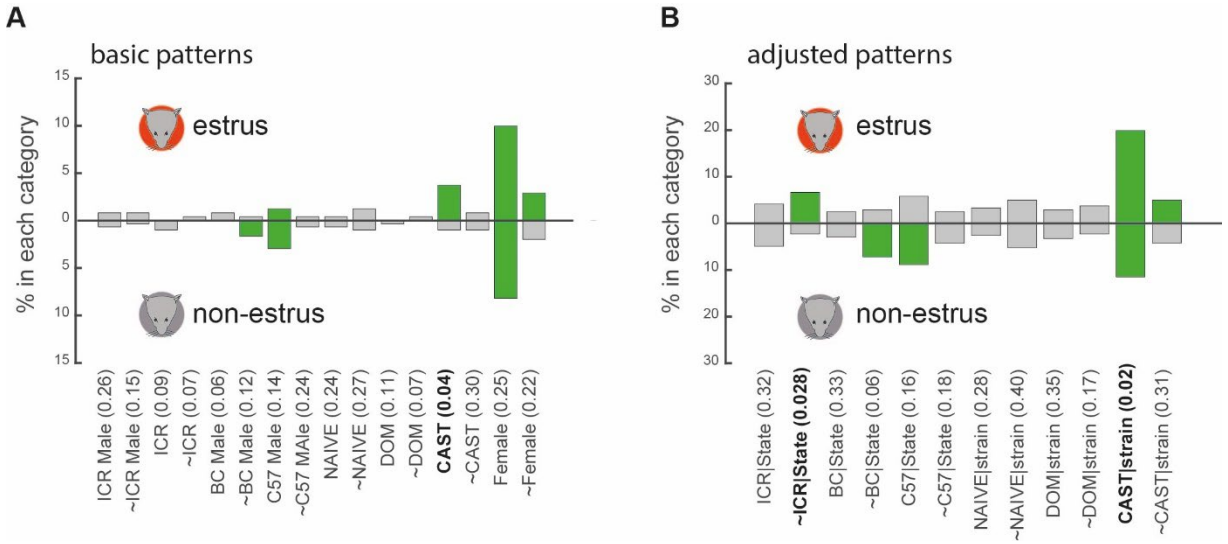

Figure 7. Comparison of response frequency under the two reproductive states. A. Frequencies of basic patterns (including complementary patterns). **B.** Frequencies of adjusted patterns (including complementary patterns). In both panels, frequencies in estrus and non-estrus females are shown above and below the horizontal axis, respectively. Significantly represented categories (using a shuffling test as described in **Fig. 3**) are indicated in green. P-values for differences for each pattern under the two states, using the binomial exact test, are listed. The Bonferroni adjusted p-values at the 0.05 level are 0.0031 (0.05/16) and 0.0042 (0.05/12), for A and B, respectively, and thus none of the differences are significant. Relaxing the correction, three categories fulfil the 0.05 criterion (indicated in bold). None of them correspond to increased representation of dominant male stimuli during estrus. Note that in some cases, a category is overrepresented only during one of the states, but this is not necessarily reflected by a significant difference among the two states (e.g., ~female).

Discussion

The first stage in sexual behavior is the appetitive stage, which is further divided to detection, approach, and investigation [2]. In rodents, the VNS is probably most important during investigation, which takes place after contact is established, allowing a thorough analysis of a potential partner's state [11, 12]. We had originally hypothesized that during estrus, responses to "virile stimuli" will be accentuated, reflecting heightened sensitivity or discriminatory ability. Instead, we found that overall, AOB representations remain stable. This conclusion is based on analysis of response magnitudes to individual stimuli and relationships between response magnitudes (**Fig. 5**), selectivity to specific stimuli (**Fig. 6**), population level representations (**Fig. 4**) and the frequency of response categories (**Fig. 7**). It is consistent with our recent observations showing representational stability in virgin and in pregnant female mice, at least under

temporal scales reflecting brief investigation bouts [43]. Combined with analysis of responses in male and female subjects [16, 46] and in males from different strains [44], we propose that the AOB conveys detailed information, but does not "interpret" it as a function of an organism's current state. Thus, the AOB provides an unbiased account of a potential partner's features, leaving evaluation of the appropriate response to downstream processing stages. Below, we first discuss what our study can reveal about response patterns of AOB neurons, and then proceed to discuss the implications for state dependent processing.

Response patterns of AOB-MCs

While the primary focus of this study was state-dependent processing, we first considered the broader topic of response properties of AOB-MCs. Chemosensory space cannot be easily parameterized like visual or auditory space, and presentation of all potential ligands (and their combinations) is clearly unfeasible. Thus, receptive fields properties of central chemosensory neurons, including AOB-MCs, are poorly characterized. The selective responses to mice from different sex and strain combinations that we observed here are consistent with previous electrophysiological [10, 16, 18, 44], and chemical analyses [47-53]. Selectivity to castrated vs. intact males has also been shown before [43], while selectivity to male dominance is consistent with chemical analyses [54] and immediate-early-gene expression profiles in the AOB [55]. Here, we asked if AOB-MC response patterns reflect behaviorally relevant features of conspecifics. We found that most response patterns (**Fig. 3**) are not more frequent than expected by chance.

We stress that we do not suggest that features such as physiological state are encoded by the activity of single neurons. In fact, we believe that most ethologically relevant features are encoded by the activity of multiple neurons. Nevertheless, such population level representations ultimately depend on the response properties of individual neurons, and we thus ask: what can we learn from our analysis of response pattern frequency? Generally, pattern frequency is determined by the fraction of molecules (or their combinations) that are common to stimuli that share some feature, and, the degree to which AOB-MCs sample these shared molecules (or their combinations). This idea is illustrated in **Fig. 8**, where for simplicity, we ignore the fact that that molecule levels are graded rather than binary, that multiple AOB-MCs can sample the same molecule, that the same molecules can be sampled by multiple AOB-MCs, and that trait selective information is often conveyed by combinations rather than single molecules. While these are critical facts, ignoring them does not alter the essence of our explanation. **Fig. 8A** represents three individuals that share a common trait (e.g., dominance), each of which emits a certain number of molecules, chosen randomly from a "world" of molecules (depicted in a 30 x 30 grid). Some of the molecules are unique to each individual (shown in in green), while others are related to the common trait and thus shared by all individuals (red). The individual-selective molecules may convey information related to individuality or to some other unrelated trait. The three rows in **Fig. 8A** represent scenarios with varying ratios between trait-selective and individual-selective molecules. Each row shows the molecules associated with each individual, as well as their union (right column).

To identify a given trait, it is needed to detect trait-selective molecules, and this involves the second element that dictates response frequency, namely the effective sampling properties of neurons (of course, AOB-MCs do not directly sample molecules, but rather VSNs, which do). Assuming some noise in production and detection of these molecules, robust trait detection should involve sampling of multiple

molecules. Given a tradeoff between robustness of detection, and redundant sampling (since resources are limited), there is likely an optimal number of molecules/neurons for the identification of any given trait. We hypothesize that tuning properties of the AOB-MC population are adapted to efficiently sample trait-selective molecules. For each trait, three scenarios are possible: non-biased sampling, over-sampling, and under-sampling of trait-selective molecules (**Fig. 8B**). Combined with the proportions of trait-selective and non-trait-selective molecules, these sampling statistics determine the frequency of particular response patterns across the population.

Taking these considerations into account, we speculate that optimal sampling by the VNS (reflecting both VNS tuning properties and AOB-MCs connectivity) involves selective sampling of rarely represented trait-related molecules, and selective avoidance of common redundant molecules. Such an organization may optimize information retrieval with limited resources, and can account for our observation that most patterns, which we assume correspond to meaningful traits, are not over-represented.

However, if sampling is optimal, why are some patterns more frequent than expected by chance? Considering male and female stimuli, there may be numerous molecules that are more prevalent in females that in males. We speculate that under-sampling can reduce, but not overcome this excess. While recent analyses indicate that only a small number of urinary molecules are unique to all males or females from different strains [47], our pattern types do not depend on unique, but rather on increased or decreased concentrations associated with specific traits. Similar considerations may apply to the C57 male category which was also over-represented in our data. Notably, analysis of chemical levels indicates that VSN selectivity for both sex and strain is less prominent than expected based on urinary contents [47]. This supports our ideas that VNS encoding acts to reduce the redundancy present in molecular levels.

The over-representation of castrated stimuli is puzzling since castrated males are not natural stimuli. Yet, this may precisely be the reason for the over-representation. Namely, if castration gives rise to sweeping changes in molecular composition, then the (hypothetical) evolutionary process of under-sampling could not happen. This would account for the puzzling fraction of castrated urine selective neurons and the strong responses to these stimuli (**Fig. 2D, E**), observed here, and elsewhere [43].

Along the same lines, in contrast to castrated stimuli, the dominant pattern was very infrequent (in fact, only one single unit in our dataset fulfilled it, **Fig. 3C**). While this is not significantly less than expected by chance, it is surprising. We note that this is not because dominant stimuli are less potent than naive stimuli; they are generally stronger (see **Fig. 2 D, E**). Nor is it likely to be due to our modest sample size, as similar pattern distributions are observed when multi-unit activity is also included in the analysis (not shown). Instead, we proposed that this scarcity may represent an optimal allocation of resources to separate dominant from naive males. Note also that population activity levels elicited by dominant and naive stimuli are similar (see **Fig. 2B**), suggesting that unlike castration, dominance is not associated with extensive chemical changes. The number of strain-adjusted dominant patterns is not negligible (**Fig. 3D**), implying that evaluation of male state might be done in the context of that male's strain. Admittedly, lacking knowledge of the chemical space associated with each of the stimuli, this and all the other ideas developed here remain speculative. A comprehensive analysis of tuning properties of AOB-MCs must take into account all the features that we ignored in our simple explanation, and consider the balance between encoding multiple traits in parallel, some of which must involve overlapping molecules.

Implications for female reproductive state dependent processing

Considering the second theme of this research, namely state dependence, our results are not at odds with multiple reports of estrus-state dependent behavioral changes in female mice. They are also reconcilable with state-dependent representations in downstream regions that reflect fluctuating hormonal states. However, our findings are unexpected in light of estrus-state dependent changes in the earlier processing stage, namely at the level of VSNs [39-41]. One possible explanation is that our approach cannot detect finer adaptations within dedicated processing streams [56]. This scenario applies in [39], which showed changes in a subset of VSNs sensitive to male stimuli. Two other studies revealed more global sex hormone dependent changes in VSNs [40, 41]. Lacking knowledge of the functional implications of such changes on the AOB network, it is difficult to explain why we did not observe broad changes. One simple possibility is that such effects will generally increase excitability. However, we did not observe such changes, perhaps due to compensatory mechanisms within the AOB. Finally, we note that despite the global stability, some of our comparisons yielded significant differences among the two states. While these differences do not represent increased (or decreased) responsiveness to virile stimuli, we cannot rule out their connection with the changes reported in VSNs.

Our experimental approach has inherent advantages and disadvantages for detecting state dependent effects. Since mice are anesthetized, changes involving active exploration or arousal cannot be detected. This includes the possible effects of feedback that may themselves be state-dependent, such as those from estrogen receptor expressing neurons in the medial amygdala [57]. On the other hand, in awake mice, there is no simple way to monitor the dynamics of stimulus uptake, which may vary with state, and thus confound state dependent neuronal responses with state dependent sampling. The anesthetized preparation ensures that stimulus uptake is consistent under both states and allows repeated delivery of multiple stimuli, regardless of the subject's engagement or motivation. In this context, we note that MOS activation using our preparation is likely minimal, thereby reducing its influence on sampling behavior, or via more direct forms of cross talk between the two systems.

In conclusion, the two themes of this study inspire two future research directions. The first calls for continued investigation of state dependent representations, in both the AOB under the awake state, and in deeper brain regions, in both anesthetized and ultimately, awake animals. The second direction involves a broader effort, to understand how behaviorally relevant features are encoded in chemical space, in early sensory processing, and eventually, decoded by downstream neurons that receive sensory inputs.

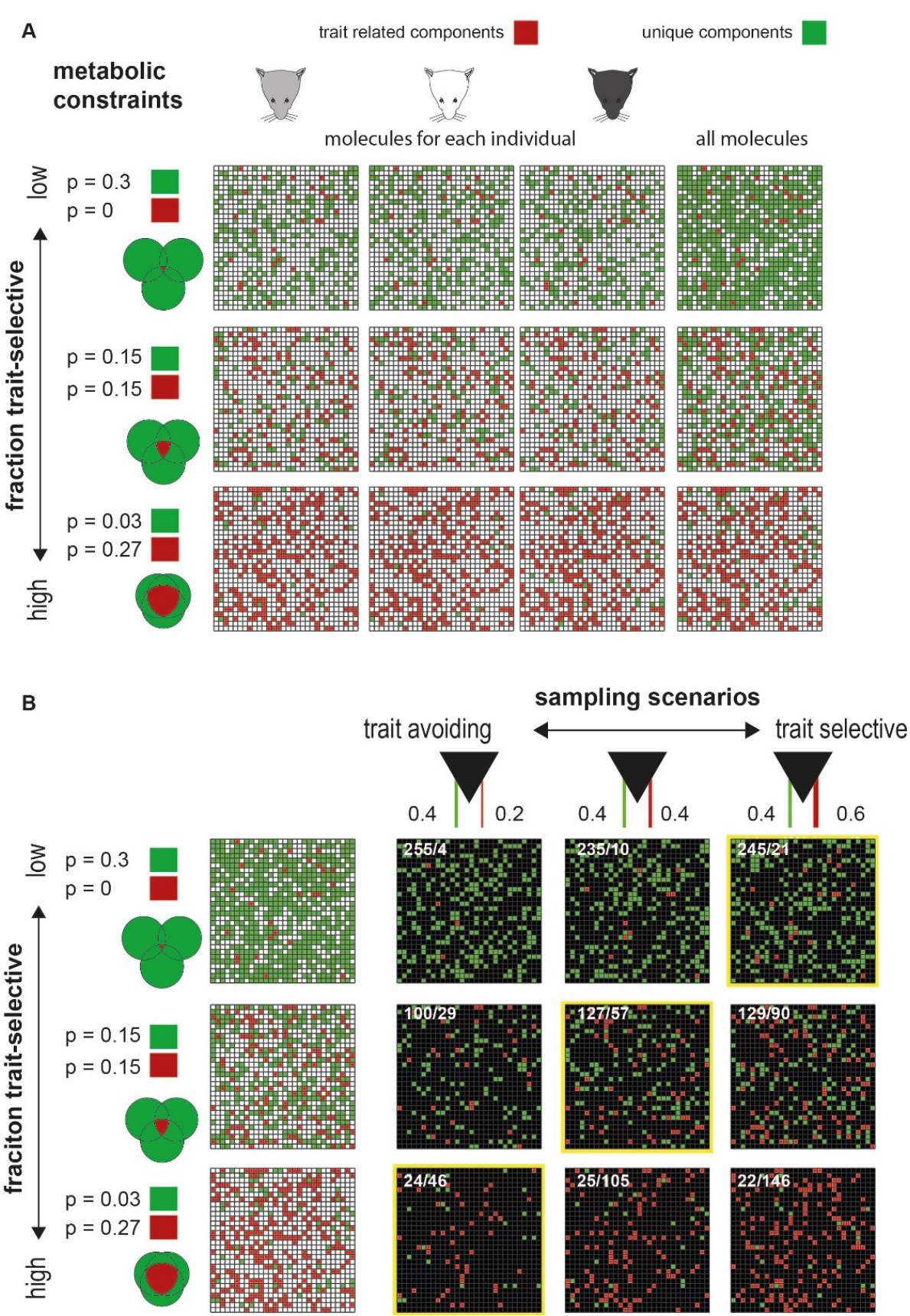
A
trait related components
unique components
metabolic constraints
molecules for each individual
all molecules
low
p = 0.3
p = 0
fraction trait-selective
p = 0.15
p = 0.15
p = 0.03
p = 0.27
high
B
sampling scenarios
trait avoiding
trait selective
0.4
0.2
0.4
0.4
0.4
0.6
fraciton trait-selective
255/4
235/10
245/21
100/29
127/57
129/90
24/46
25/105
22/146

Figure 8. Schematic illustration of sampling of trait selective molecules. A. Molecular profiles associated with three individuals sharing a common trait. Trait selective molecules are shown in red and all others (unique molecules) are shown in green, within a 30 x 30 grid representing all (900) molecules in the world. The three individuals are indicated on the three columns on the left. The rightmost column shows their union. Rows correspond to different proportions of individual specific and trait selective molecules. **B.** Different sampling scenarios by AOB neurons. The three rows correspond to the scenarios shown in A. The left column is the union of all molecules under each scenario, as shown in A. The three other columns represent sampling schemes that differ in the proportion of trait selective vs. other molecules sampled, moving from trait avoiding, to balanced, to trait selective sampling. The two values above each column indicate the probability of sampling unique (left), or common (trait-selective) molecules (right). We speculate that sampling properties are matched to component frequencies, thereby balancing robustness of trait detection with redundancy. We note that receptive fields of AOB-MCs are actually determined by VSNs and by their interactions with AOB-MCs.

Materials and Methods

Subjects

For recordings, we used sexually unexperienced adult female mice from the ICR strain (Envigo Laboratories, Israel). All experiments complied with the Hebrew University Animal Care and Use Committee.

Determination of the estrus stage

Female estrus stage was determine using a vaginal lavage of 15 ul of saline. The saline sample was then deposited on a Superfrost plus slide (Thermo Scientific), and dried. Slides were treated with Wright Stain Solution (Sigma), and photographed under a light microscope. The estrus stage was determined using the cytological composition of the smear, as described in [58, 59].

Male status

Our stimulus set includes urine samples from castrated, naive, and dominant proven breeder mice. Proven breeder and naive male mice were purchased (Envigo Laboratories, Israel) and then assigned to cages containing two proven breeders and 2-3 naive mice. One to two days after mice were placed in these cages, we identified candidate dominant male (always one of the two proven breeders) by observation of their home cages. To confirm dominance, we conducted dominance tests involving each proven breeder mouse with each of the other cage mates (including all naive cage-mates and the other proven breeder male). The test included a "tube test", conducted in a new cage with clean bedding. The two mice were placed at opposite ends of a cylindrical tube and the mouse that forced the other to exit was designated as dominant. In addition, immediately following this tube test, the same pair of mice was monitored for an additional 10 minutes, and the mouse displaying aggressive behavior (biting, chasing, tail rattling) towards the other was identified as dominant. We only classified mice as dominant if they showed dominance during the tube test and the subsequent observation period in the cage. We also confirmed that the established hierarchy was maintained throughout the entire period of urine collection, over the course of ~4 weeks, by monitoring the behavior of these mice in their home cages. Dominant male mice consistently showed aggressive behaviors, whereas non-dominant mice engaged in self grooming behaviors more frequently. Castrated male urine was collected from 8-weeks old males that had their testes removed under Isoflurane anesthesia at the age of 4 weeks (before puberty).

Stimuli and dataset

Stimuli were collected from castrated, naive, and sexually experienced male mice from the BALB/C, C57BL/6 and ICR strains and estrus and non-estrus sexually-naive adult female mice from the ICR strain (Envigo Laboratories, Israel). For urine collection, mice were gently held over a plastic sheet until they urinated. The urine was collected in plastic tubes, flash-frozen in liquid nitrogen, and then stored at -80°C. Each of the samples presented here comprised urine from 3 different individuals, diluted 1:10 in Ringer's solution. Urine from each individual was collected over a period of ~ 4 weeks and pooled before combining it with urine from males of the same strain and status.

Surgical procedures and electrode positioning

Experimental procedures were detailed in [60]. Briefly, mice were anesthetized with 100mg/kg ketamine and 10mg/kg xylazine, tracheotomized, and a cuff electrode was implanted around the sympathetic nerve trunk. Incisions were closed with Vetbond (3M) glue, and the mouse was placed in a stereotaxic apparatus where anesthesia was maintained throughout the experiment (0.5-1% isoflurane in oxygen). A craniotomy was made immediately rostral to the rhinal sinus, the dura was removed, and electrodes were advanced

into the AOB at an angle of ~30° with an electronic micromanipulator (MP-285; Sutter Instruments, Novato, CA). We used 32 channel probes (NeuroNexus Technologies, Ann Arbor, Michigan) with 8 channels on each of 4 shanks, with the following specification: (horizontal) distance between the shanks: 200µm, site area: 177 μm^2, and (vertical) within-shank site spacing either 50µm or 100µm (NeuroNexus acute probe models: A4x8-5mm-100-200-177-A32 and A4x8-5mm-50-200-177-A32). Before recordings, electrodes were dipped in fluorescent dye (DiI, Invitrogen, Carlsbad, CA) to allow subsequent confirmation of placement within the AOB external cellular layer (ECL).

Stimulus presentation procedure

Each session contains several distinct stimuli. Typically, each stimulus was presented repeatedly in a pseudorandom order, at least 4 times, and typically 5 times within each session across all sessions (number of repeated presentations per stimulus: 5.1± 0.9, mean ± sd. In 72% of the cases, stimuli were given 5 or more times. Otherwise, they were presented 4 times). Stimuli were presented in blocks, and within each block all stimuli were presented in a random order. An inter-trial interval of 18s was applied between stimulus presentations. During each presentation, 2 µl of stimulus were manually applied directly into the nostril using a micropipette [60]. After a delay of 20 s, a square-wave stimulation train (duration: 1.6 s, current: ±120 µA, frequency: 30 Hz), was delivered through the sympathetic nerve cuff electrode to induce vomeronasal organ suction. Following another 40 s delay, the nasal cavity was flushed with 1-2ml of ringer's solution, and drained with suction from the nasopalatine duct. The cleansing procedure lasted 50 s and included sympathetic trunk stimulation to facilitate stimulus elimination from the vomeronasal organ lumen.

Electrophysiology

Neuronal data was recorded using an RZ2 processor, PZ2 preamplifier, and two RA16CH head-stage amplifiers (TDT, Alachua, FL). Single-unit and multi-unit activity were sampled at 24414 Hz and band-pass filtered at 300-5000 Hz. Custom MATLAB codes were used to extract spike waveforms. Spikes were sorted automatically according to their projections on two principal components on 8 channels of each shank using KlustaKwik [61, 62] and then manually verified and adjusted using Klusters [62]. Spike clusters were evaluated by their waveforms, projections on principal component space (calculated for each session individually) and autocorrelation functions. A cluster was defined as a single-unit if it displayed a distinct spike shape, was fully separable from both the origin (noise) and other clusters, and if its autocorrelation function demonstrated a clear trough around time 0 of at least 10 ms. Clusters apparently comprising more than one single-unit were designated as multi-units. Under these definitions, multi-units could represent the activity of as few as two units. Such units are not included in our dataset. As a further criterion for single-unit classification, we examined the "shape symmetry" of all spike shapes. Shape symmetry was defined as the correlation coefficient of the two sides (margins) of the spike waveform around its peak (in absolute value, with one of the margins reversed). For example, if the waveform contains 9 samples with a peak at sample 5, the correlation will be calculated between the vectors defined by samples 1-4 and a reversed version of the vector defined by samples 6-9. If the shape is symmetric, the symmetry will be 1. When the peak is not in the middle, as is usually the case, the correlation is calculated for vectors determined by the smaller margin. A high symmetry (>0.95) is helpful for identifying noise accidentally misclassified as spikes. Using a graphical representation of all spike shapes, we examined the entire data set for such noise-like spikes and removed them from further analyses.

Data analysis

All data analyses and visualizations were performed using custom and built-in MATLAB code. The response of a unit to a given stimulus was defined as the average firing rate change over a 60 s window following stimulus application (change measured compared to the 17 s period preceding application). This broad

response window covers both the post application and post stimulation periods, as in [44]. This window was chosen because in some cases, responses began after stimulus application, and prior to electric stimulation of the SNT. Response significance of a given unit to a given stimulus was determined by comparing its spiking rate distribution following all repeats to the baseline firing frequency distribution during the 17 s period prior to stimulus application. Response significance (of a particular unit to a given stimulus) was determined by a non-parametric analysis of variance (*kruskalwallis* test) comparing the set of post-stimulation rates to the set of preceding baseline rates (preceding rates were pooled across all stimuli), using a threshold of 0.05. In the image in **Fig. 2A** (and in other related representations), the response magnitude of each unit was normalized by the absolute value of the maximal response (i.e., the response to the stimulus that elicited the strongest response, in absolute value). Thus, all response values range between -1 and 1. In addition, in this image and in some analyses, all non-significant responses were set to 0. For **Fig. 2B**, we applied classical multi-dimensional scaling, using the data in each of the rows in **Fig. 2A**, using the MATLAB *cmdscale* function, and the *correlation* distance metric (defined as one minus the sample correlation).

In a preliminary stage of analysis, we sought to define response patterns according to response significance (for example, with a dominant pattern implying that all dominant stimuli elicit significant responses, while all other stimuli do not). However, this approach yielded a very small number of neurons conforming to each pattern. Thus, we ultimately applied more permissive criteria. These criteria rely on relative response magnitudes, as shown in **Fig. 3A**. For example, an ICR male pattern (upper row in left the matrix in **Fig. 3A**) is fulfilled by neurons whose responses to each of the three ICR male stimuli are *stronger* than responses to all of the other stimuli (regardless of response significance). In the complementary pattern (~ICR male, shown in the upper row in central matrix), the response to each of these stimuli must be *smaller* than to all the other stimuli. As one example of a strain adjusted pattern, to qualify for a dominant/strain pattern, a neuron's response to the dominant stimulus must be stronger than responses to all other male stimuli from the same strain. In other words, strain (or state) adjusted patterns involve three distinct conditions, as shown in the right panel of **Fig. 3A**. Note that the adjusted patterns involve more permissive criteria than the non-adjusted patterns. Thus, for example, a dominant pattern, is by definition also a strain-adjusted dominant pattern (dominant/strain).

To analyze pattern frequencies, for each pattern, we first found the number of neurons that conform to each of the patterns. Then, we calculated the probability to observe that number of cases by "chance". To analyze if response frequencies occur more often than expected by chance, we constructed a null distribution by shuffling the response data matrix. In this matrix, (as in **Fig. 2A**), each row corresponds to one neuron, and each column corresponds to one stimulus. In each of 100,000 iterations, we randomly shuffled the order of all elements within a column, and calculated the frequency of each response pattern. This frequency for each pattern was calculated across all iterations, allowing us to evaluate the probability to obtain the observed frequencies given only the marginal probabilities to each stimulus.

To correlate global response similarity between neurons recorded in estrus and non-estrus female, we used the MATLAB *pdist* function, which calculates pairwise distances along arrays. The arrays in our cases were the population responses (after normalization, as shown in the matrices in **Fig. 4A**). We used the *correlation* and *Euclidean* distance measures for **Fig. 4B, D** and **Fig. 4C**, **E** respectively. We used the MATLAB *corrcoef* function to calculate the correlation coefficient and the p-value (the probability to observe such a large correlation under the hypothesis of no correlation).

To calculate significance of differences in the number of neurons responding under each of the two states (**Fig. 5A**), we tested the null hypothesis that response probability is identical under both states. This was done by calculating the observed probability (based on the total number of responding neurons, per stimulus, across both states), and then calculating four different probabilities under the binomial distribution: the probability to obtain the observed number or more responding neurons in estrus, the probability to obtain the observed number or less of responding neurons in estrus, and the corresponding probabilities for neurons recorded in non-estrus females. The smallest (i.e., most unlikely) value of these four probabilities was then considered as the p-value. Since the smallest p-value is taken, this yields a sensitive test of differences. To calculate significance of differences between mean response magnitudes for each stimulus (**Fig. 5B**), we used a two-tailed non-parametric analysis of variance (*kruskalwallis* test), comparing the distributions of response strengths across all neurons recorded in estrus and in non-estrus females. A Bonferroni correction for multiple corrections was applied. For two-way ANOVA we used the MATLAB *anovan* function, with stim identity, and female state as factors, using a *full* model.

The pairwise preference index PI_{AB} for two stimuli A and B, (as shown in **Fig. 5C**), is defined as $(R_A-R_B) / (R_A + R_B)$, where R_A and R_B are the responses to stimulus A and B after rectification (i.e., after setting negative responses to zeros). Rectification was applied to keep the range of the preference indices between -1 and 1. For each pair of stimuli, we only considered neurons that showed a significant response to at least one of the stimuli. Then, the mean preference indices were calculated for each stimulus pair, as shown in **Fig. 5C**, for neurons recorded in estrus and non-estrus females. The correlation coefficient and p-value were derived using the *corrcoef* MATLAB function, as described above.

To compare pairwise preference indices across states (**Fig. 5D, E**), we also used a bootstrapping approach. Specifically, we first found the absolute difference between the mean preference indices for a given stimulus pair under the two states. Then, we repeatedly shuffled the data set (effectively, neurons were randomly assigned to one of the two reproductive states) 100,000 times, and calculated the absolute difference across the two (shuffled) states. Then, we derived the p-values as the fraction of cases in the shuffled distribution which were larger than the actual observed distribution. In other words, these p-value reflect the probability to obtain such a state-dependent difference in preference indices by chance.

To calculate lifetime sparseness (S), we used the definition given in [63]:

$$S = \left[1 - \frac{(\sum_i |r_i|/N)^2}{\sum_i (r_i^2)/N}\right] \Big/ \left[1 - \frac{1}{N}\right]$$

Where r_i is the response of neuron to the ith stimulus (averaged across all trials) and N is the number of stimuli (N=11 in our case). S varies between 0 and 1, with 0 indicating uniform responses to all stimuli and 1 indicating a response to only one stimulus. Lifetime sparseness distributions across states were compared using a non-parametric analysis of variance (*kruskalwallis*).

Triangles plots in **Fig. 6B** were generated by considering the response of each neuron to each of three stimuli. Negative responses were truncated to 0 in this analysis. The position of each point is determined by the relative weights of three unit vectors pointing from the triangle center to each of the three vertices. The selectivity index (**Fig. 6C**) was calculated for each neuron (and each stimulus triplet) as in [46]. Specifically, it is the normalized distance from the center of the triangle, with values ranging between 0 (lowest selectivity, center of triangle), and 1 (highest selectivity, vertices of the triangles).

$$Si = \frac{\sqrt{(a-m)^2 + (b-m)^2 + (c-m)^2}}{d}$$

where a, b, and c are the responses to each of three stimuli. The value corresponding to equal responses to all stimuli is m, which is equal to 1/3. d is the maximum possible value of the numerator of the equation, and is equal to $\sqrt{2/3}$. Selectivity index distributions under the two states were compared using a non-parametric analysis of variance (*kruskalwallis*).

For comparison of category frequency distributions under the two states (**Fig. 7A, B**), we applied a binomial exact text under the hypothesis of equal distributions under two states. Essentially, we followed the same procedure described above for comparing the number of responsive neurons, with the difference that here we calculated the probability to obtain a certain number of neurons corresponding to each pattern. Bars in **Fig. 7** are shaded in green if the probability to obtain the observed pattern frequency (calculated separately for each state), is smaller than 0.05, employing the same shuffling approach described for **Fig. 3C**.

All the raw data, processed data, and codes will be provided by the authors upon request.

Tables

Significant median differences in mean responses between stimulus pairs, with Tukey Kramer correction for multiple comparisons

```
M_ICR_NAIVE vs M_ICR_CAST          p: 0.042255
M_ICR_NAIVE vs M_C57_CAST          p: 0.015033
M_ICR_NAIVE vs F_ICR_NON_EST       p: 0.0010519
M_ICR_NAIVE vs F_ICR_EST           p: 0.037127
M_ICR_CAST  vs M_BC_NAIVE          p: 0.0052463
M_BC_NAIVE  vs M_C57_CAST          p: 0.0014844
M_BC_NAIVE  vs F_ICR_NON_EST       p: 6.5788e-05
M_BC_NAIVE  vs F_ICR_EST           p: 0.004468
M_BC_DOM    vs F_ICR_NON_EST       p: 0.045776
```

Significant median differences in mean responses between stimulus pairs without correction for multiple comparisons

```
M_ICR_NAIVE vs M_ICR_CAST          p: 0.0010636
M_ICR_NAIVE vs M_C57_CAST          p: 0.00033956
M_ICR_NAIVE vs F_ICR_NON_EST       p: 2.0771e-05
M_ICR_NAIVE vs F_ICR_EST           p: 0.00091914
M_ICR_DOM   vs M_ICR_CAST          p: 0.030301
M_ICR_DOM   vs M_C57_CAST          p: 0.013284
M_ICR_DOM   vs F_ICR_NON_EST       p: 0.001636
M_ICR_DOM   vs F_ICR_EST           p: 0.027304
M_ICR_CAST  vs M_BC_NAIVE          p: 0.00011046
```

```
M_ICR_CAST  vs M_BC_DOM          p: 0.023567
M_ICR_CAST  vs M_C57_DOM         p: 0.033367
M_BC_NAIVE  vs M_BC_CAST         p: 0.025458
M_BC_NAIVE  vs M_C57_NAIVE       p: 0.046268
M_BC_NAIVE  vs M_C57_CAST        p: 2.9626e-05
M_BC_NAIVE  vs F_ICR_NON_EST     p: 1.2366e-06
M_BC_NAIVE  vs F_ICR_EST         p: 9.3289e-05
M_BC_DOM    vs M_C57_CAST        p: 0.010052
M_BC_DOM    vs F_ICR_NON_EST     p: 0.0011646
M_BC_DOM    vs F_ICR_EST         p: 0.021159
M_BC_CAST   vs F_ICR_NON_EST     p: 0.008915
M_C57_NAIVE vs M_C57_CAST        p: 0.029007
M_C57_NAIVE vs F_ICR_NON_EST     p: 0.0042801
M_C57_DOM   vs M_C57_CAST        p: 0.014786
M_C57_DOM   vs F_ICR_NON_EST     p: 0.001865
M_C57_DOM   vs F_ICR_EST         p: 0.030109
```

Table 1. Comparison of stimulus response magnitudes across stimulus pairs (related to Fig. 2E). The tests were conducted using a non-parametric ANOVA (kruskalwallis), and the multcompare MATLAB function with the Tukey Kramer multiple comparisons correction (top), or without correction (bottom).

Type of comparison	Stimulus 1	Stimulus 2	Non-estrus Selectivity	Estrus selectivity	Selectivity score p-value
Female vs. female	F ICR estrus	F ICR non estrus	**0.53788 (169)**	0.49684 (142)	0.34024
Male vs. female	ICR dom	ICR estrus	0.71497 (175)	**0.74204 (141)**	0.99068
	ICR dom	ICR non estrus	0.73335 (171)	**0.75566 (156)**	0.82341
	ICR naïve	ICR estrus	0.72123 (175)	**0.73349 (136)**	0.81005
	ICR naïve	ICR non estrus	0.69395 (166)	**0.74774 (147)**	0.26472
Different states for a given strain	ICR dom	ICR naïve	**0.60467 (138)**	0.57776 (115)	0.43316
	C57 dom	C57 naïve	**0.66205 (150)**	0.46707 (110)	3.9015e-05
	BC dom	BC naïve	**0.62197 (137)**	0.56784 (103)	0.25603
	ICR dom	ICR cast	0.67063 (166)	**0.73886 (154)**	0.33714
	C57 dom	C57 cast	**0.71072 (194)**	0.6357 (127)	0.064372
	BC dom	BC cast	**0.73796 (155)**	0.72499 (147)	0.63383
	ICR naive	ICR cast	0.66641 (159)	**0.71219 (144)**	0.3776
	C57 naïve	C57 cast	**0.6886 (180)**	0.59994 (132)	0.02337
	BC naïve	BC cast	**0.76303 (155)**	0.75291 (145)	0.49453
Different strains for a given virility state	C57 naïve	BC naive	**0.63828 (131)**	0.62625 (114)	0.60412
	C57 naïve	ICR naive	**0.64574 (139)**	0.60728 (117)	0.47299
	BC naïve	ICR naïve	**0.60711 (134)**	0.53642 (101)	0.089909
	C57 dom	BC dom	**0.68609 (152)**	0.62328 (108)	0.096686
	C57 dom	ICR dom	**0.71036 (157)**	0.62786 (118)	0.039544
	BC dom	ICR dom	**0.66277 (147)**	0.56956 (114)	0.036236
	ICR cast	BC cast	**0.70931 (169)**	0.58111 (157)	0.00097307

	ICR cast	C57 cast	**0.67162 (199)**	0.60862 (147)	0.10409
	BC cast	C57 cast	**0.71471 (190)**	0.58251 (144)	0.0009967

Table 2. Detailed comparison of selectivity for pairs of stimuli between estrus and non-estrus neurons (Related to Fig. 6). p-values are calculated using a non-parametric ANOVA (kruskalwallis). Significant differences after adjustment for 23 comparisons (0.05/23 = 0.0022) are shown in red. Significant differences without adjustment (at the 0.05) are shown in blue. For each stimulus pair, values for the state with the higher selectivity are shown in bold font. The number of neurons in each comparison is indicated in parenthesis in the corresponding selectivity columns.

Acknowledgements

We thank Michal Yoles-Frenkel, Anat Kahan, and Karen Marom for help and support throughout this project. We thank Dr. Annika Cichy for helpful comments on the text. This work was supported by the Israeli Science Foundation (ISF) grant (1703/16).

References

1. Lenschow, C. and S.Q. Lima, *In the mood for sex: neural circuits for reproduction.* Curr Opin Neurobiol, 2020. **60**: p. 155-168.
2. Yin, L. and D. Lin, *Neural control of female sexual behaviors.* Horm Behav, 2023. **151**: p. 105339.
3. Zinck, L. and S.Q. Lima, *Mate choice in Mus musculus is relative and dependent on the estrous state.* PLoS One, 2013. **8**(6): p. e66064.
4. Gutierrez-Castellanos, N., et al., *Neural and behavioral plasticity across the female reproductive cycle.* Trends Endocrinol Metab, 2022. **33**(11): p. 769-785.
5. Nelson, R.J. and L.J. Kriegsfeld, *An introduction to behavioral endocrinology*. Sixth edition. ed. 2022, New York: Oxford University Press/Sinauer Associates. xii, 672 pages.
6. Liberles, S.D., *Mammalian pheromones.* Annu Rev Physiol, 2014. **76**: p. 151-75.
7. Spehr, M., et al., *Parallel processing of social signals by the mammalian main and accessory olfactory systems.* Cell Mol Life Sci, 2006. **63**(13): p. 1476-84.
8. Mohrhardt, J., et al., *Signal detection and coding in the accessory olfactory system.* Chem Senses, 2018.
9. Hamacher, C., et al., *A revised conceptual framework for mouse vomeronasal pumping and stimulus sampling.* Curr Biol, 2024. **34**(6): p. 1206-1221 e6.
10. Luo, M., M.S. Fee, and L.C. Katz, *Encoding pheromonal signals in the accessory olfactory bulb of behaving mice.* Science, 2003. **299**(5610): p. 1196-201.
11. Keller, M., et al., *The main and the accessory olfactory systems interact in the control of mate recognition and sexual behavior.* Behav Brain Res, 2009. **200**(2): p. 268-76.
12. Keller, M., et al., *The vomeronasal organ is required for the expression of lordosis behaviour, but not sex discrimination in female mice.* Eur J Neurosci, 2006. **23**(2): p. 521-30.

13. Oboti, L., et al., *A wide range of pheromone-stimulated sexual and reproductive behaviors in female mice depend on G protein Galphao.* BMC Biol, 2014. **12**: p. 31.
14. Doyle, W.I., et al., *Faecal bile acids are natural ligands of the mouse accessory olfactory system.* Nat Commun, 2016. **7**: p. 11936.
15. Kahan, A. and Y. Ben-Shaul, *Extracting Behaviorally Relevant Traits from Natural Stimuli: Benefits of Combinatorial Representations at the Accessory Olfactory Bulb.* PLoS Comput Biol, 2016. **12**(3): p. e1004798.
16. Ben-Shaul, Y., et al., *In vivo vomeronasal stimulation reveals sensory encoding of conspecific and allospecific cues by the mouse accessory olfactory bulb.* Proc Natl Acad Sci U S A, 2010. **107**(11): p. 5172-7.
17. Hendrickson, R.C., et al., *Inhibition shapes sex selectivity in the mouse accessory olfactory bulb.* J Neurosci, 2008. **28**(47): p. 12523-34.
18. Tolokh, II, X. Fu, and T.E. Holy, *Reliable sex and strain discrimination in the mouse vomeronasal organ and accessory olfactory bulb.* J Neurosci, 2013. **33**(34): p. 13903-13.
19. Hellier, V., et al., *Female sexual behavior in mice is controlled by kisspeptin neurons.* Nat Commun, 2018. **9**(1): p. 400.
20. Moncho-Bogani, J., et al., *Attractive properties of sexual pheromones in mice: innate or learned?* Physiol Behav, 2002. **77**(1): p. 167-76.
21. Martinez-Ricos, J., et al., *Intraspecific communication through chemical signals in female mice: reinforcing properties of involatile male sexual pheromones.* Chem Senses, 2007. **32**(2): p. 139-48.
22. Coopersmith, C.B. and S. Lenington, *Female Preferences Based on Male Quality in House Mice - Interaction between Male-Dominance Rank and T-Complex Genotype.* Ethology, 1992. **90**(1): p. 1-16.
23. Martinez-Ricos, J., et al., *Role of the vomeronasal system in intersexual attraction in female mice.* Neuroscience, 2008. **153**(2): p. 383-95.
24. Rokni, D. and Y. Ben-Shaul, *Object-oriented olfaction: challenges for chemosensation and for chemosensory research.* Trends Neurosci, 2024.
25. Takami, S. and P.P. Graziadei, *Light microscopic Golgi study of mitral/tufted cells in the accessory olfactory bulb of the adult rat.* J Comp Neurol, 1991. **311**(1): p. 65-83.
26. Larriva-Sahd, J., *The accessory olfactory bulb in the adult rat: a cytological study of its cell types, neuropil, neuronal modules, and interactions with the main olfactory system.* J Comp Neurol, 2008. **510**(3): p. 309-50.
27. Mossman, C.A. and L.C. Drickamer, *Odor preferences of female house mice (Mus domesticus) in seminatural enclosures.* J Comp Psychol, 1996. **110**(2): p. 131-8.
28. McCarthy, E.A., et al., *Effect of Ovarian Hormones and Mating Experience on the Preference of Female Mice to Investigate Male Urinary Pheromones.* Chem Senses, 2018. **43**(2): p. 97-104.
29. Moncho-Bogani, J., et al., *Attraction to male pheromones and sexual behaviour show different regulatory mechanisms in female mice.* Physiol Behav, 2004. **81**(3): p. 427-34.
30. Nomoto, K. and S.Q. Lima, *Enhanced male-evoked responses in the ventromedial hypothalamus of sexually receptive female mice.* Curr Biol, 2015. **25**(5): p. 589-94.
31. Yin, L., et al., *VMHvll(Cckar) cells dynamically control female sexual behaviors over the reproductive cycle.* Neuron, 2022. **110**(18): p. 3000-3017 e8.
32. Inoue, S., et al., *Periodic Remodeling in a Neural Circuit Governs Timing of Female Sexual Behavior.* Cell, 2019. **179**(6): p. 1393-1408 e16.
33. Wang, L., R.A. DeFazio, and S.M. Moenter, *Excitability and Burst Generation of AVPV Kisspeptin Neurons Are Regulated by the Estrous Cycle Via Multiple Conductances Modulated by Estradiol Action.* eNeuro, 2016. **3**(3).

34. McHenry, J.A., et al., *Hormonal gain control of a medial preoptic area social reward circuit.* Nat Neurosci, 2017. **20**(3): p. 449-458.
35. Dias, I.C., et al., *The Structural and Electrophysiological Properties of Progesterone Receptor-Expressing Neurons Vary along the Anterior-Posterior Axis of the Ventromedial Hypothalamus and Undergo Local Changes across the Reproductive Cycle.* eNeuro, 2021. **8**(3).
36. Christensen, A., P. Dewing, and P. Micevych, *Membrane-initiated estradiol signaling induces spinogenesis required for female sexual receptivity.* J Neurosci, 2011. **31**(48): p. 17583-9.
37. Knoedler, J.R., et al., *A functional cellular framework for sex and estrous cycle-dependent gene expression and behavior.* Cell, 2022. **185**(4): p. 654-671 e22.
38. Liu, M., et al., *Encoding of female mating dynamics by a hypothalamic line attractor.* Nature, 2024.
39. Dey, S., et al., *Cyclic Regulation of Sensory Perception by a Female Hormone Alters Behavior.* Cell, 2015. **161**(6): p. 1334-44.
40. Cherian, S., et al., *Estradiol rapidly modulates odor responses in mouse vomeronasal sensory neurons.* Neuroscience, 2014. **269**: p. 43-58.
41. Eckstein, E., et al., *Cyclic regulation of Trpm4 expression in female vomeronasal neurons driven by ovarian sex hormones.* Mol Cell Neurosci, 2020. **105**: p. 103495.
42. Stowers, L. and S.D. Liberles, *State-dependent responses to sex pheromones in mouse.* Curr Opin Neurobiol, 2016. **38**: p. 74-9.
43. Yoles-Frenkel, M., et al., *The Bruce effect: Representational stability and memory formation in the accessory olfactory bulb of the female mouse.* Cell Rep, 2022. **40**(8): p. 111262.
44. Bansal, R., et al., *Do all mice smell the same? Chemosensory cues from inbred and wild mouse strains elicit stereotypic sensory representations in the accessory olfactory bulb.* BMC Biology, 2021. **19**(1): p. 133.
45. Nodari, F., et al., *Sulfated steroids as natural ligands of mouse pheromone-sensing neurons.* J Neurosci, 2008. **28**(25): p. 6407-18.
46. Bergan, J.F., Y. Ben-Shaul, and C. Dulac, *Sex-specific processing of social cues in the medial amygdala.* Elife (Cambridge), 2014. **3**: p. e02743.
47. Nagel, M., et al., *Deciphering the chemical language of inbred and wild mouse conspecific scents.* Elife, 2024. **12**.
48. Fu, X., et al., *A Molecular Code for Identity in the Vomeronasal System.* Cell, 2015. **163**(2): p. 313-23.
49. Cheetham, S.A., et al., *Limited variation in the major urinary proteins of laboratory mice.* Physiol Behav, 2009. **96**(2): p. 253-61.
50. Schwende, F.J., et al., *Urinary volatile constituents of the house mouse,Mus musculus, and their endocrine dependency.* J Chem Ecol, 1986. **12**(1): p. 277-96.
51. Albone, E.S. and S.G. Shirley, *Mammalian semiochemistry : the investigation of chemical signals between mammals*. 1984, Chichester West Sussex ; New York: Wiley. xii, 360 p.
52. Lin da, Y., et al., *Encoding social signals in the mouse main olfactory bulb.* Nature, 2005. **434**(7032): p. 470-7.
53. Zhang, J.X., et al., *Putative chemical signals about sex, individuality, and genetic background in the preputial gland and urine of the house mouse (Mus musculus).* Chem Senses, 2007. **32**(3): p. 293-303.
54. Thoss, M., et al., *Regulation of volatile and non-volatile pheromone attractants depends upon male social status.* Sci Rep, 2019. **9**(1): p. 489.
55. Veyrac, A., et al., *The main and accessory olfactory systems of female mice are activated differentially by dominant versus subordinate male urinary odors.* Brain Res, 2011. **1402**: p. 20-9.

56. Ishii, K.K., et al., *A Labeled-Line Neural Circuit for Pheromone-Mediated Sexual Behaviors in Mice.* Neuron, 2017. **95**(1): p. 123-137 e8.
57. Inbar, T., R. Davis, and J.F. Bergan, *A sex-specific feedback projection from aromatase-expressing neurons in the medial amygdala to the accessory olfactory bulb.* J Comp Neurol, 2021.
58. Byers, S.L., et al., *Mouse estrous cycle identification tool and images.* PLoS One, 2012. **7**(4): p. e35538.
59. Caligioni, C.S., *Assessing reproductive status/stages in mice.* Curr Protoc Neurosci, 2009. **Appendix 4**: p. Appendix 4I.
60. Yoles-Frenkel, M., et al., *In vivo stimulus presentation to the mouse vomeronasal system: Surgery, experiment, setup, and software.* J Neurosci Methods, 2017. **285**: p. 19-32.
61. Csicsvari, J., et al., *Massively parallel recording of unit and local field potentials with silicon-based electrodes.* J Neurophysiol, 2003. **90**(2): p. 1314-23.
62. Hazan, L., M. Zugaro, and G. Buzsaki, *Klusters, NeuroScope, NDManager: a free software suite for neurophysiological data processing and visualization.* J Neurosci Methods, 2006. **155**(2): p. 207-16.
63. Vinje, W.E. and J.L. Gallant, *Sparse coding and decorrelation in primary visual cortex during natural vision.* Science, 2000. **287**(5456): p. 1273-6.